Journal of Materials Chemistry C

ARTICLE

Engineering the singlet-triplet energy splitting in a TADF molecule

Paloma L. Santos,*[a] Jonathan S. Ward,[b] Przemyslaw Data, [a] Andrei S. Batsanov, [b] Martin R. Bryce, [b] Fernando B. Dias [a] and Andrew P. Monkman [a]

Received 00th January 20xx,
Accepted 00th January 20xx

DOI: 10.1039/x0xx00000x

www.rsc.org/

The key to engineering an efficient TADF emitter is to achieve a small energy splitting between a pair of molecular singlet and triplet states. This work makes important contributions towards achieving this goal. By studying the new TADF emitter 2,7-bis(phenoxazin-10-yl)-9,9-dimethylthioxanthene-*S,S*-dioxide (DPO-TXO2) and the donor and acceptor units separately, the available radiative and non-radiative pathways of DPO-TXO2 have been identified. The energy splitting between singlet and triplet states was clearly identified in four different environments, in solutions and solid state. The results show that DPO-TXO2 is a promising TADF emitter, having ΔE_{ST} = 0.01 eV in zeonex matrix. We further show how the environment plays a key role in the fine tuning of the energy levels of the ^{1}CT state with respect to the donor ^3LE_D triplet state, which can then be used to control the ΔE_{ST} energy value. We elucidate the TADF mechanism dynamics when the ^{1}CT state is located below the ^{3}LE triplet state which it spin orbit couples to, and we also discuss the OLED device performance with this new emitter, which shows maximum external quantum efficiency (E.Q.E) of 13.5% at 166 cd/m^2 .

Introduction

The efficiency and brightness of organic light emitting diodes (OLEDs) have been improved extensively since these devices were discovered. In 1987 Tang and Van Slyke, who produced the first bilayer OLED, reported an external quantum efficiency of 1%. In contrast, in 2014, Yirang Im and Jun Yeob Lee fabricated an OLED with external quantum efficiency above 20%.[1,2] This massive improvement results directly from many years of investigation into methods to overcome the limitation imposed by spin statistics in the charge recombination mechanism, i.e. the fact that three times more triplet excitons than singlet excitons are generated in OLEDs, when the injected charge carriers recombine to give excitons. This leads to a considerable loss on the internal efficiency of OLEDs, because triplet excitons are in general not emissive at room temperature, and thus only the singlet excitons directly contribute to the OLED`s emission. Recently, thermally activated delayed fluorescence (TADF) has become a viable method to convert triplet excitons into emissive singlet states. This mechanism uses thermal energy to up-convert the lower energy triplet excitons (dark states) into emissive singlet states of higher energy, thereby surpassing the imposed 25% internal quantum efficiency.[3–8]

The TADF mechanism relies on thermal energy to raise the triplet state to a vibronic sub level that is isoenergetic with the emissive singlet states by enabling reverse intersystem crossing (RISC), an energy conserving process. Therefore, the energy splitting between the singlet and triplet states (ΔE_{ST}) plays a key role in the TADF emitters. In order to maximize TADF, ΔE_{ST} should be minimized. This has been achieved by designing organic molecules that show intramolecular excited states with strong charge transfer character (CT). Normally, these molecules have a minimal spatial overlap between the highest occupied and lowest unoccupied molecular orbitals, HOMO and LUMO respectively, and thus achieve very small exchange energy (J) leading to a very small ΔE_{ST}. [9]

The discovery of new TADF emitters, which are more efficient and with higher stability, requires suitable electron donor (D) and electron acceptor (A) units, with the appropriate ionization potential (IP) and electron affinity (EA) to achieve minimal ΔE_{ST} in the CT-TADF emitter. However, while the tuning of the IP and EA levels is necessary, it is not sufficient to maximize TADF. Other requirements are also important, as for example (i) suppressing the internal conversion pathways available for the singlet and triplet excited states, in order to maximize emission yields, given that with minimal interaction between ground and excited state in the CT manifold, the radiative decay time will be long, and (ii) the engineering of molecular geometries, to minimize the electron coupling between the DA units, to achieve excited states with strong CT character, as for example in TADF emitters with near orthogonal DA units. Further work is still necessary to fully understand how the efficiency of the TADF mechanism can be controlled, so more efficient emitters can be designed.

As mentioned above, one strategy that has been implemented to achieve minimal singlet triplet energy splitting is to design DA molecules with subunits restricted in a near orthogonal position, i.e. with a large dihedral angle between their planes.[10–12] In this arrangement, the electronic coupling between the D and A subunits is in principle very small, which increases the CT character and thus minimizes ΔE_{ST}. However, this arrangement may also influence the mechanisms of intersystem crossing. Spin orbit coupling (SOC) for example is formally forbidden between singlet and triplet CT states for the case of near orthogonal D and A units, and thus the ^{1}CT state can only couple strongly to a close lying local triplet state. [13,14] The gap between these two states is thus the real ΔE_{ST} that requires thermal energy for triplets to cross over to the singlet state. These means that ^{1}CT can be either above or below the coupling triplet state for TADF to occur, but needs to be close to a local triplet state, so efficient SOC can occur. Intersystem crossing between the singlet and triplet excited states can however occur by hyperfine coupling

[a] Physics Department, Durham University, South Road, Durham DH1 3LE, UK
[b] Department of Chemistry, Durham University, South Road, Durham DH1 3LE, UK

†Electronic Supplementary Information (ESI) available: Synthetic details; copies of NMR spectra; additional photophysical and OLED data; CV data; CCDC reference number 1426131.

See DOI: 10.1039/x0xx00000x

(HFC), but the energy difference between the singlet and triplet CT states has to be very small, i.e. when the electronic coupling between ^{1}CT and ^{3}CT is weak.[15] Therefore, the roles of SOC and HFC on the TADF mechanism may be decisive to define the best energy ordering of the singlet and triplet excited states to maximize TADF.

Experimental and theoretical studies have compared TADF molecules with different structures; donor-acceptor type (D-A type) and donor-acceptor-donor type (D-A-D type). The subsequent results show that D-A-D displays more efficient TADF, and higher photoluminescence quantum yields (PLQY) versus their analogues D-A. [16,17] For this reason, we have synthesised the 2,7-bis(phenoxazin-10-yl)-9,9-dimethylthioxanthene-*S,S*-dioxide (DPO-TXO2), a D-A-D TADF emitter formed by phenoxazine (D) donors and the 9,9-dimethylthioxanthene-*S,S*-dioxide (TXO2) (A) acceptor. Phenoxazine was chosen because of its strong electron donor character, due its low ionization potential, and because it assumes a near D-A orthogonal structure. Moreover, phenoxazine has been less extensively explored when compared with carbazole and fluorene in OLED materials. [18–22] To the best of our knowledge, this is the first time that the dimethyl TXO2 acceptor unit has been incorporated into a D-A-D molecule: it has a strongly folded and constrained structure which is in contrast to the very flexible diphenylsulfone[23] and the planar and rigid dibenzothiophene-*S,S*-dioxide units,[5] which are both well-established in TADF molecules. In comparison with dibenzothiophene-*S,S*-dioxide, the conjugation between the two phenyl rings of TXO2 is disrupted by the dimethylmethylene bridge. The dimethyl groups were added to prevent any deprotonation at the bridging carbon.

Here, we report the photophysical properties of DPO-TXO2 and its subunits in detail to unravel the influence of molecular geometry, and the order of electronic states on the efficiency of the TADF mechanism. The results show that DPO-TXO2 is a promising TADF emitter, having a small ΔE_{ST} in different environments, in solutions and solid state. We show that the environment can be used to control the ΔE_{ST} energy value and, also, we elucidate the TADF mechanism dynamics when the ^{1}CT state is located below the ^{3}LE triplet state with which it interacts by spin orbit coupling. The folded TXO2 acceptor yields a high triplet energy and also a shallow LUMO level which affects electron transport and injection into the emitter molecules in an OLED device necessitating a radical change to the device architecture.

Experimental

The synthesis and structural characterization of DPO-TXO2 as well as the acceptor unit (9,9-dimethylxanthene-*S,S*-dioxide) are given in detail in the supplementary information (S1, ESI†). Phenoxazine was purchased from Sigma Aldrich.

Three types of samples were studied in this work: solutions in different solvents (10^{-3} to 10^{-5} M), film produced in zeonex matrix (organic material 5 mg/mL : zeonex 180 mg/mL 1:1 v/v) and thin film produced in CBP matrix (10% DPO-TXO2:CBP). All the solutions were diluted in different solvents and stirred for 24 hours. They also were degassed to remove all the oxygen dissolved in the solutions by 4 freeze-thaw cycles to perform the degas test and delayed fluorescence measurements. The films in zeonex matrix were fabricated by spin-coating on quartz substrates at 500 rpm during 60 seconds. The thin film in a CBP matrix was made by co-evaporation deposition onto transparent sapphire substrates using a Kurt J. Lesker Spectros II deposition system under vacuum, 10^{-6} mbar, at a steady evaporation rate of ~ 2.3 Å/ s and ~ 0.22 Å/ s for host and guest materials, respectively.

Steady state absorption and emission spectra were acquired using a UV-3600 Shimadzu spectrophotometer and a Jobin Yvon Horiba Fluoromax 3, respectively. Time resolved spectra were obtained by exciting the sample with a Nd:YAG laser (EKSPLA), 10 Hz, 355 nm/266 nm or by using a Nitrogen laser, 10 Hz, 337 nm. For Nd:YAG laser and Nitrogen laser the earliest emission available for collection were at time delay (TD) at 1 ns and 30 ns, respectively. Sample emission was directed onto a spectrograph and gated iCCD camera (Stanford Computer Optics).

OLED devices were fabricated using pre-cleaned indium-tin-oxide (ITO) coated glass substrates purchased from Ossila with a sheet resistance of 20 Ω/cm^2 and ITO thickness of 100 nm. The OLED devices had a pixel size of 4 mm by 4 mm. The small molecule and cathode layers were thermally evaporated using the Kurt J. Lesker Spectros II deposition chamber at 10^{-6} mbar.

Results and discussion

The chemical structure and the single-crystal X-ray molecular structure of DPO-TXO2 are shown in figure 1. The molecule has no crystallographic symmetry, and an approximate non-crystallographic mirror plane through S(1), O(1), O(2), C(7), C(14) and C(15). The arene rings *A* and *B* of the acceptor form a dihedral angle of 137.8°. The twists around the N(1)-C(4) and N(2)-C(10) bonds, 89.9° and 73.2°, preclude significant intramolecular conjugation. The phenoxazine substituent at C(10) is folded along the N(2)…O(4) vector, while the phenoxazine substituent at C(4) is twisted. The dihedral angle between arene rings *C* and *D* equals 173.3°, that between *E* and *F* is 162.2°. The bonds N(1)-C(16) and N(1)-C(22) in the more planarised phenoxazine unit average 1.400(2) Å, bonds N(2)-C(28) and N(2)-C(34) in the more puckered one average 1.415(2) Å, while the non-conjugated bond distances N(1)-C(16) and N(1)-C(22) average 1.434(2) Å. The HOMO-LUMO levels of DPO-TXO2 and its donor and acceptor units were investigate by cyclic voltammetry (CV) analyses (Fig. S2, ESI†) and found to be at $HOMO_{DPO\text{-}TXO2}$= -5.37 eV - $LUMO_{DPO\text{-}TXO2}$=-2.61 eV, $HOMO_D$= -5.15 eV, $LUMO_A$=-2.33 eV . Consistent with the extensive twisting around the N(1)-C(4) and N(2)-C(10) bonds in the X-ray molecular structure, the CV data confirms that the HOMO and LUMO levels are largely localized on the donor and acceptor units, respectively, as observed in other D-A-D type molecules. This feature identifies DPO-TXO2 as a promising molecule for TADF; the near orthogonality of the D and A components results in very small exchange energy and singlet-triplet energy gap. This feature should facilitate the activated RISC, leading to efficient TADF if the CT level is degenerate with a local triplet state.

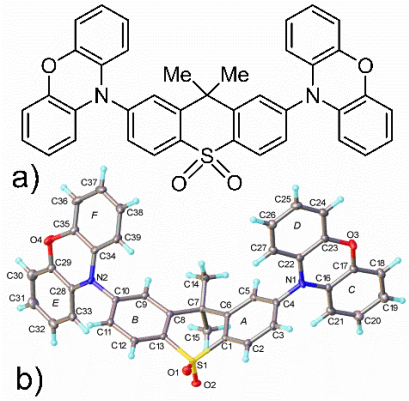

Fig. 1 a) Chemical structure and b) X-ray molecular structure of DPO-TXO2: thermal ellipsoids are drawn at 50% probability level.

Solution state properties

Figure 2 shows the normalized optical absorption spectra of the acceptor (A) and donor (D) units as well as DPO-TXO2 molecule, measured in dilute methyl cyclohexane (MCH) solvent. The inset of figure 2 shows the absorption peak around 390 nm in different solvents. In the DPO-TXO2 absorption spectrum, the first two absorption peaks (higher energy) also exist in the absorption spectra region of A and D molecules. The third peak, around 390 nm, does not appear neither in the D nor the A absorption spectra. It shows a slight red shift by increasing the polarity of the solvent, which is associated with π → π* transitions. We assigned this peak to the CT absorption in the D-A-D molecule. This is a relatively strong transition confirming its π-π* character.

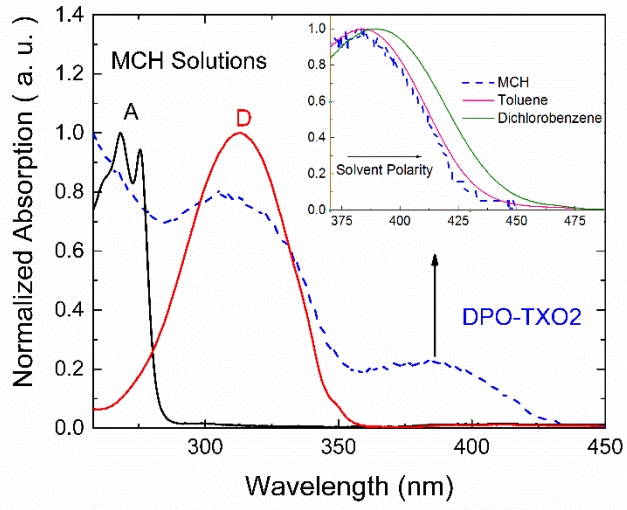

Fig. 2 Optical absorption spectra of the acceptor (A), donor (D), and DPO-TXO2 molecules, all diluted in methyl cyclohexane (MCH) solvent. Inset graph - absorption spectra peak around 390 nm of DPO-TXO2 in different solvents.

Figure 3 shows the normalized photoluminescence (PL) spectra of DPO-TXO2, and of the D and A single units, all in MCH solution with excitation around their absorption peak. Also in figure 3, the inset shows the PL spectra of DPO-TXO2 in solvents of increasing polarity, showing a strong positive solvatochromism. Both the emission peak and full width at half maximum (FWHM) increase dramatically with solvent polarity. The DPO-TXO2 molecule emits blue light in MCH and green/yellow in dichlorobenzene. In the three solvents studied, the DPO-TXO2 PL spectra show clear and strong CT emission, evidenced by their Gaussian band shape and red shift compared to the individual D and A spectra. In the less polar solvent (MCH), a blue shifted emission peaking around 370 nm is also observed and is assigned to residual donor emission (^1LE_D). This result shows that in MCH the radiative recombination from ^1LE_D can compete with electron transfer that populates the ^1CT state, indicating the weak electronic coupling between the donor ^1LE_D state and the molecular CT state. When DPO-TXO2 is excited at any of its three distinct absorption regions, the emission always arises from the CT state, indicating that the charge transfer occurs by excitation of the donor and the acceptor units. In other words, there is symmetry in the charge transfer process and hole and electron transfer give rise to the same CT emission (Fig. S3, ESI†).

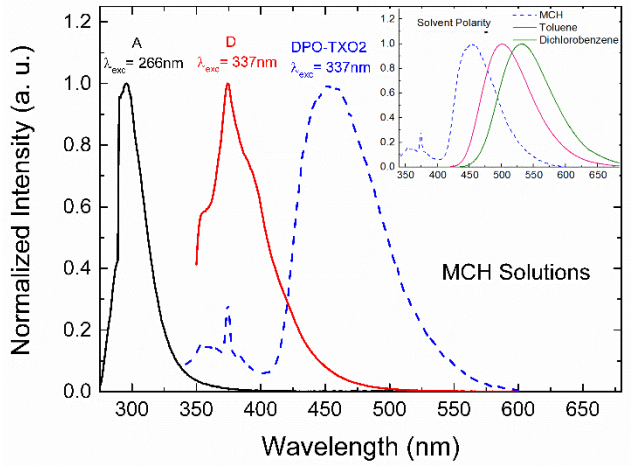

Fig. 3 Normalized photoluminescence (PL) spectra of acceptor (A), donor (D), and DPO-TXO2 molecules, all diluted in MCH solvent. Inset graph - PL of DPO-TXO2 in different solvents.

After showing that the DF contribution in DPO-TXO2 is strongly dependent on the polarity of the medium (inset graph fig.3) within which the emitter is dispersed, we proceeded to investigate the causes of this strong influence by studying different environments.

The delayed fluorescence in MCH solution was studied with the aim to investigate an environment where the DPO-TXO2 has weaker ion pair character in the CT state, i.e. the state retains strong local excited state character. The contribution of triplet excited states to the overall emission was determined by comparing the emission intensity in aerated and degassed solutions (Fig. S4, ESI†). The emission spectra obtained in degassed and non-degassed solutions match each other, showing that DF and prompt fluorescence come from the same ^1CT state. The CT emission increases by a factor of 3.10 when oxygen is removed, thus the contribution of delayed fluorescence is 52%.

Figure 4a shows the decay curve of DPO-TXO2 in MCH solution from the early prompt emission (TD = 1.1 ns) to the end of the DF (TD = 0.14 ms), at different temperatures. The curves were obtained with 355 nm excitation. The decay curves are complex, prompt and delayed emission regions are not well defined, but the DF emission has clearly higher intensity at high temperatures, indicating TADF. The analyses of the normalized spectra (Fig.4b) in the entire region of study shows that at early times the emission spectra observed match the ^1LE_D emission of the donor. It is possible to identify the two regimes of the donor emission, a peak around 375 nm identified in the steady state measurements, and a dimer emission, peak around 450 nm, that can be seen just in the iCCD measurements. Increasing the time delay, the emission spectra progressively shift to longer wavelengths, moving from the ^1LE_D emission to stabilized ^1CT emission, passing through a region where both, ^1LE_D and CT emission, are observed, showing very slow electron transfer. At TD = 14.9 ns the CT emission is clearly observed and has onset at (2.94 ± 0.02) eV. However, the emission shows a slight red shift at very late times, indicating a contribution from donor phosphorescence (PH). After TD = 0.8 µs, the PH emission is stabilized with onset at (2.78 ± 0.02) eV, and was collected until 0.14 ms. The observed triplet emission comes from the localized triplet state of the donor or/and the acceptor. Thus, we investigated the localized triplet states (^3LE) of the donor and acceptor, studying these units separately. The ^3LE_D phosphorescence of the donor was found to have onset at (2.79 ± 0.02) eV in toluene solution, corroborating with the PH spectra obtained for DPO-TXO2, and also, with the triplet levels of phenoxazine reported previously in other solvents. [24] The PH spectra of the acceptor unit was found to have onset at (3.39 ± 0.02) eV, higher energy than the PH of DPO-TXO2. Thus, the triplet emission observed in DPO-TXO2 clearly comes from the donor units. Thus, the

^{1}CT state and the ^3LE_D state were identified in a MCH solution, and the splitting between these states was found to be ΔE_{ST} = (0.16± 0.03) eV.

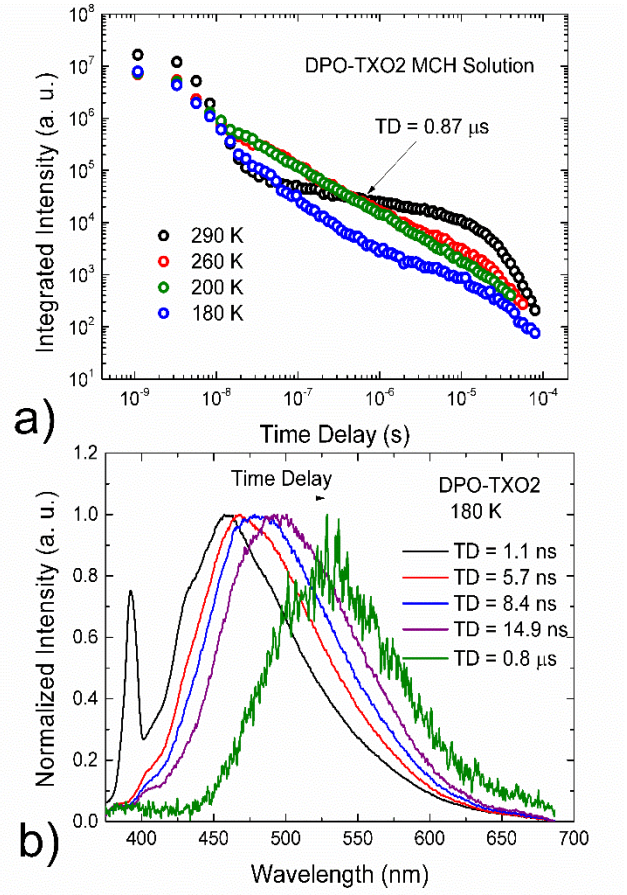

Fig. 4 a) Time resolved fluorescence decay of DPO-TXO2 in MCH solution. The curves were obtained with 355 nm excitation. b) Time resolved normalized emission spectra in the entire region of analyses.

The delayed fluorescence in toluene solution was also studied since it was demonstrated to be a stable environment for CT emission of DPO-TXO2. The contribution of DF to the overall emission in DPO-TXO2 was found to be 4.8 or 82% (Fig. S5, ESI†), indicating a much strong ion pair character to the CT state.

Figure 5 shows the decay curve of DPO-TXO2 in toluene solution. There is a clear bi-exponential decay with a fast component of τ_{PF} =24.8 ns, assigned to the prompt fluorescence component (^{1}CT), and a longer decay of τ_{DF} = 4.61 µs, assigned to the delayed fluorescence component. The curve was obtained with 355 nm excitation. When τ_{DF} is short, exciton annihilation processes such as triplet-triplet annihilation (TTA) are expected to be supressed. Also the ratio between I_{DF} and I_{PF}, the integral of DF and PF regions, respectively, was calculated and found to be $\bar{n}$ = 4.81 , where $\bar{n}$ is emission contribution of TADF, in excellent agreement with the value calculated by the degassing test in toluene solution ($\bar{n}$= 4.80). From this, the reverse intersystem crossing rate constant was determined using equation 1 and shown to be 1.04 x10^6 s^{-1} .[5]

$$k_{RISC} = \frac{\int I_{DF}(t)dt}{\int I_{PF}(t)dt} \cdot \frac{1}{\tau_{DF}} \quad (1)$$

Figure 6a shows the decay curve of DPO-TXO2 toluene solution at different temperatures. The curves were obtained with 337 nm excitation. The decay curves of the DPO-TXO2 show clearly four distinct regions, delineated by three well-defined crossing points: 51 ns, 5.6 µs and 63 µs. The decay below 51 ns, is dominated by ^{1}CT→S_0 prompt fluorescence, and between 51 ns and 63 µs is the ^{1}CT→S_0 delayed fluorescence that dominates, and ^3LE_D→S_0 phosphorescence is also clearly observed in the region from 63 µs to 1 ms.

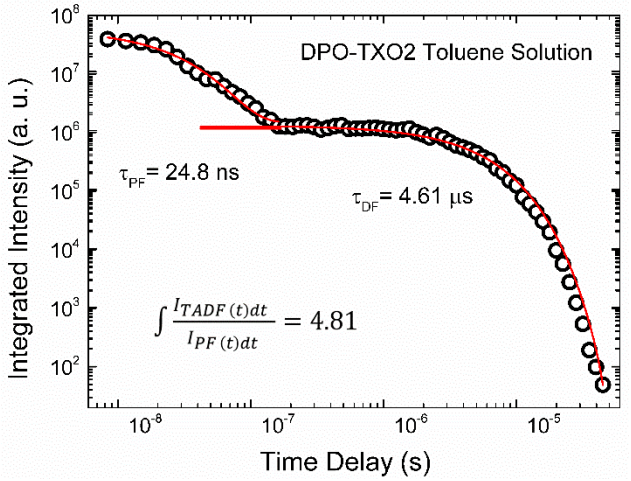

Fig. 5 Time resolved fluorescence decay of DPO-TXO2 molecules in toluene solution. The curve was obtained with 355 nm excitation.

The decay curves at different temperatures show that the prompt region increases in emission intensity on cooling down the system, and at 180 K the onset of DF occurs at later times. In region A, the DF emission increases in intensity with increasing temperature, in concordance with the TADF mechanism, because of the increase in the available thermal activation energy. The intensity dependence of the DF emission in this region was analysed as a function of the laser excitation dose, and a linear gradient of 1.045 ± 0.005 was found (Fig. S6, ESI†). This result confirms the thermally assisted mechanism as opposed to triplet-triplet annihilation (TTA). Region B has an inverse temperature dependence, the intensity of the emission again increases as the system temperature drops. The DF intensity dependence spectra as a function of excitation dose in this region also shows a linear gradient (1.025 ± 0.004) (Fig. S7, ESI†), confirming that this region also has a thermally assisted mechanism. The behaviour of the temperature dependence in this region is unexpected and can be understood by analyses of the triplet lifetime (τ_T), given by equation 2,

$$\tau_T = \frac{1}{k_{RISC} + k_T} \quad (2)$$

where K_{RISC} is the constant of RISC process and k_T is the sum of non-radiative and radiative triplet decays. At high temperature, $K_{RISC} >> k_T$, and the triplet lifetime is τ_T . At low temperature, k_{RISC} and k_T decreases, due to their temperature dependence, and, consequently, τ_T increases, making the decay curve of DPO-TXO2 longer lived so phosphorescence occurs with higher efficiency at longer times where TADF no longer occurs. Hence, we can see a crossing point at TD = 56 µs in the decay curves at different temperatures indicating the turning point in this TADF/phosphorescence competition. Also, it should be mentioned that the dielectric constant of toluene slightly increases with decreasing the temperature.[25] Hence, at lower temperature, the CT state is slightly lower energetically, leading to an increased ΔE_{ST}, and consequently, longer triplet lifetime. Region C shows the longest

lived component of the decay curve. This appears just at low temperatures, vanishing at room temperature, and is assigned to the long lived ^3LE_D phosphorescence (PH).

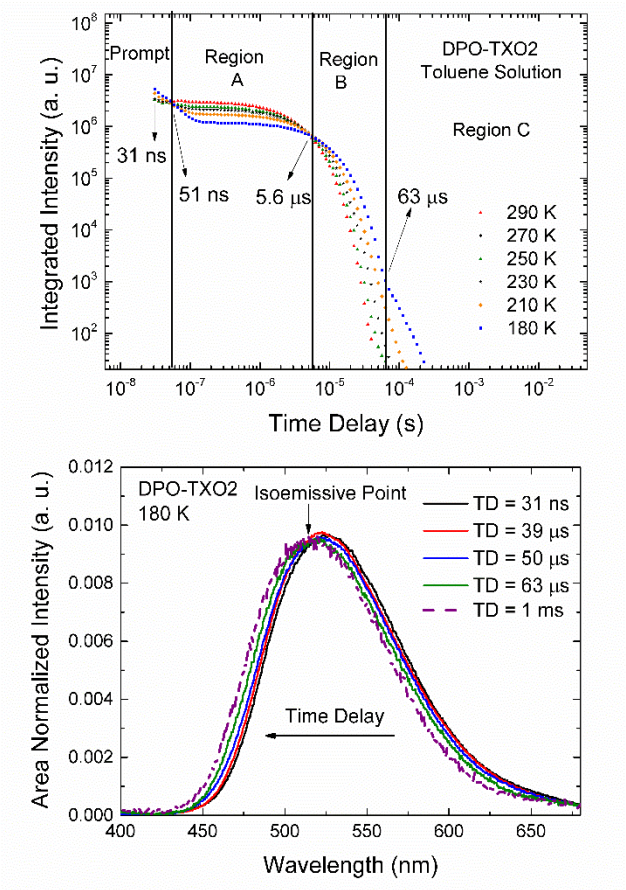

Fig. 6 a) Time resolved fluorescence decay of DPO-TXO2 molecules in toluene solution in different temperatures. The curves were obtained with 337 nm excitation. b) Time resolved area normalized emission spectra in the entire region of analyses.

Figure 6b shows the area normalized emission spectra at 180 K, giving the peak position of each spectrum. From TD = 31 ns to 39 µs, all the spectra have the same position, onset at (2.70±0.02) eV, and same spectral shape. From TD = 39 µs to 63 µs a very slight and continuous blue shift is observed, due to the growing contribution of the ^3LE_D phosphorescence. The prompt and DF emission, until TD = 63 µs, have almost identical spectral shape, showing that both originate from the same singlet excited state. Finally, after 63 µs the spectra achieve onset at (2.77±0.02) eV and the same emission was collected until TD = 1 ms. The isoemissive point (identified in Fig 6.b) gives a clear indication for the presence of two excited state species, firstly the ^1CT state and then a triplet state. The PH emission has onset very close to that found in MCH solution (2.78 ± 0.02) eV, showing that the phosphorescence of the donor does not change in different solvents. Thus, the ^1CT state and the ^3LE_D state were identified in a DPO-TXO2 toluene solution, and the splitting between these states was found to be ΔE_{ST} = (0.07 ± 0.03) eV. Additionally, the activation energy (E_A) required for the DF process was calculated from an Arrhenius fit of the temperature dependent DF emission intensity and found to be E_A = (0.031 ± 0.005) eV, in agreement with this ΔE_{ST} value. However, E_A depends of the molecule`s conformation and may be not exactly equal to ΔE_{ST}.

Comparing both environments, we observed that in toluene solution the contribution of delayed fluorescence is higher than in MCH solution, 82% and 52%, respectively. This is a direct consequence of the larger ΔE_{ST} in MCH solution. Also, the lifetime of the DF in MCH is clearly longer than in toluene, due to the larger ΔE_{ST}, corroborating other TADF emitters.[26] It is important to notice, that the ^3LE_D energy level in MCH and in toluene solutions differs by just (0.01± 0.02) eV, and the ^1CT energy levels change considerably with solvent polarity, causing a big difference in the energy splitting according to the environment. Therefore, the environment has a strong influence on the ΔE_{ST} energy value.

Figure 7 shows the full decay pathways available in DPO-TXO2 molecules dispersed the two different environment, MCH and toluene solutions. All the energy levels were taken from the onset of the spectra at 180 K in degassed solutions. Upon optical excitation of the donor or acceptor units, the population of ^1CT states are formed by electron or hole transfer. Intersystem crossing (direct and reverse) occurs between ^1CT and ^3LE_D, and the energy splitting between them is strongly dependent of the polarity of the system, mainly because of the strong solvatochromism experienced by the ^1CT state. The mechanism responsible for the delayed fluorescence in both cases is TADF. In MCH solution, ^3LE_D is located below ^1CT, excitons in the triplet levels must gain energy to match the singlet levels and then crossing the states, considering that RISC/ISC processes are adiabatic transitions. On the other hand, in toluene solution, ^3LE_D is located above the ^1CT, this is an unusual situation, but not a forbidden one as the excitons come from different states. In this environment, the ^1CT state is the level where excitons that gain thermal energy and match the ^3LE_D triplet states results in ISC, a result observed for first time in a TADF emitter. In this case, one would expect the DF to decrease as this ^1CT 'quenching channel' decreases with a concomitant increase in the prompt ^1CT emission, as we clearly observe. This also explains the later onset of DF at 180 K as well.

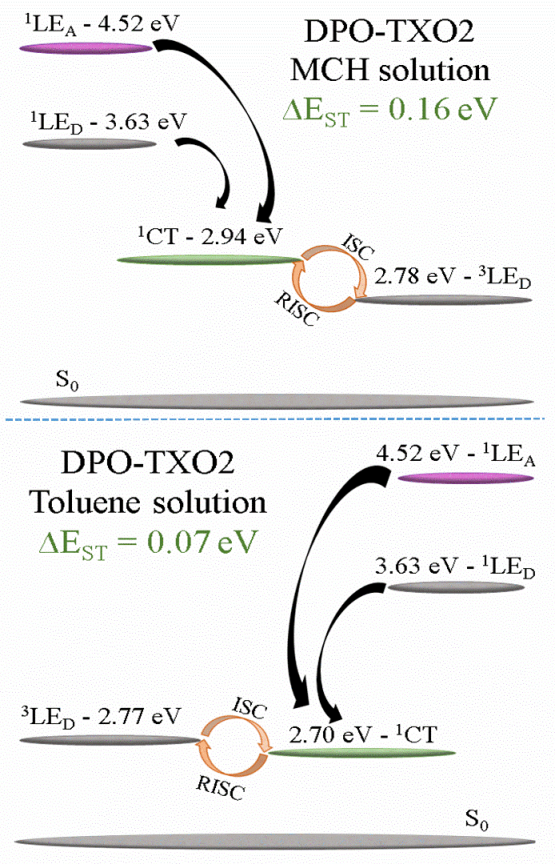

Fig. 7 Energy levels diagram describing the excited dynamics of DPO-TXO2 in Toluene and MCH solutions, evidencing the localized and charge transfer states.

Solid state properties

The TADF mechanism of DPO-TXO2 in solid-state was also studied. Figure 8 shows PL of the acceptor and donor units as well as DPO-TXO2, all as films dispersed in zeonex matrix. The PL spectrum of the acceptor shows the main emission of the unit, peak at 300 nm, and also a weak emission around 475 nm, which may be associated with a dimer emission. By time resolved spectroscopy the dimer emission was accentuated and identified to have onset at 2.98 eV. The PL of DPO-TXO2 molecule shows a clear CT emission, as well as a small contribution from donor emission. This is similar behavior to that observed in the steady state spectra of DPO-TXO2 in MCH solution (Fig.3). The similarity of the optical behaviour between these two samples is expected as both are non-polar environments.

Figure 9a shows the decay curves of DPO-TXO2 in zeonex matrix. The well-defined separation between prompt and delayed emission is observed just at 290 K, whereas at lower temperature these two distinct emissions are unclear. Emission spectra detected in the long time delay region were observed just at low temperature, indicating that, in this region, the emission comes from triplet states. Figure 9b shows the normalized spectra collected in the whole region of analyses. At early times, from TD = 1.1 ns to 18 ns, the spectra show the same emission of the donor unit dispersed in zeonex film, which continuously red shifts to higher wavelengths until it achieves the CT state emission, onset at (2.83 ± 0.02) eV. The initial donor emission is weak, only being detected with the iCCD measurements. From TD = 70 µs to 89 ms the phosphorescence spectrum is observed to have an onset at (2.84 ± 0.02) eV. The PH spectrum is undoubtedly the ^{3}LE state from the donor, matching with the PH spectrum identified by the donor units in zeonex matrix, onset at (2.83 ±0.02) eV. Also, the intensity dependence of the DF spectra (TD = 30 µs) was analysed as a function of the laser excitation dose and a linear gradient of (0.99 ± 0.03) was found, confirming the thermally assisted mechanism. Therefore, the ^{1}CT state and the ^3LE_D state were identified in a DPO-TXO2 zeonex film, and the energy splitting between these states was found to be ΔE_{ST} = (0.01 ± 0.03) eV. Additionally, the activation energy required for the DF process, again calculated from an Arrhenius fit, was found to be E_A = (0.031 ± 0.004) eV, in agreement with ΔE_{ST} value.

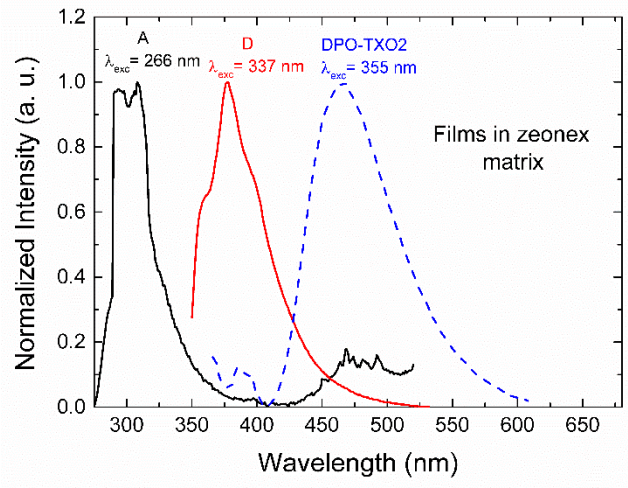

Fig. 8 Normalized photoluminescence (PL) spectra of acceptor (A), donor (D), and DPO-TXO2 molecules, all dispersed in zeonex matrix.

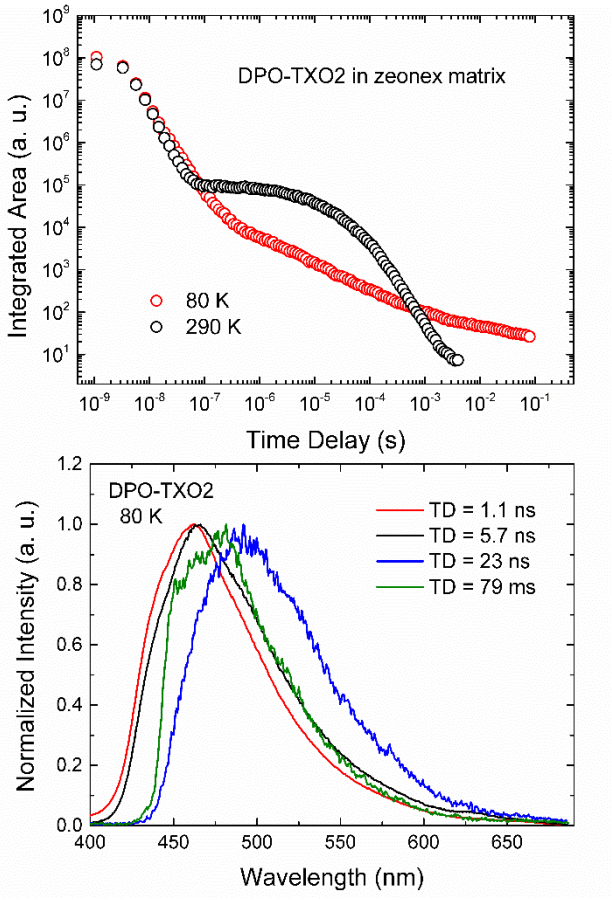

Fig. 9 a) Time resolved fluorescence decay of DPO-TXO2 in zeonex matrix. The curves were obtained with 355 nm excitation. b) Time resolved normalized emission spectra in the entire region of analyses.

The second solid state environment chosen was 4,4′-bis(*N*-carbazolyl)-1,1′-biphenyl (CBP), because CBP is a host material with relatively higher triplet level used in OLED emitter layers. However, often host–guest interactions give rise to complex photophysics, such as emissive exciplex states or quenching of excitons by the host.[4] Figure 10a shows the decay curves of the DPO-TXO2 in CPB matrix at two different temperatures. The well-defined separation between prompt and delayed emission is observed just at 290 K, at low temperature these two distinct emissions are unclear, as observed in the zeonex film (Fig.9a). Figure 10b shows the normalized emission spectra recorded at different time delays, from the early prompt emission (TD = 5.7 ns) to the phosphorescence emission (TD = 89 ms). From TD = 5.7 ns to TD = 72.5 ns, the spectra show a slight and continuous red shift, due to a growing contribution from a phosphorescence component. After TD = 72 ns, the spectra remain at 2.66 eV (onset) and this emission was collected until 89 ms. The PH spectra identified at long TD is clearly the PH of the host, CBP, having three well defined peaks (at 491 nm, 518 nm and 557 nm) with increasing emission intensity on cooling down the system.[27,28] In this thin film, the excited states were not confined on the DPO-TXO2 molecules, and a quenching of fluorescence was observed by the host. Therefore, the ^{1}CT was identified to be at 2.82 eV and the ^1LE_D level was not identified. Obviously, the ^1LE_D level must have energy higher than 2.66 eV in this environment, otherwise the phosphorescence of the CBP would not be a favourable pathway of decay and we would identify the ^1LE_D level. Also, the ^1LE_D in this film should be close to the one found in zeonex matrix, as the observed

triplet energy difference in toluene and MCH solutions is negligible. As we clearly observe TADF and a strong DF component at high temperature, we surmise that in fact the ^3LE_D is most likely lower in energy than the ^1CT state so at high temperature RISC out competes triplet transfer from guest to host whereas at 80 K the RISC rate is much lower and triplet energy transfer out competes the TADF. This could well be a consequence of the nature of the more dense small molecule host CBP compared to the polymer host zeonex. Hence, this would suggest a $\Delta E_{ST} \leq 0.13$ eV.

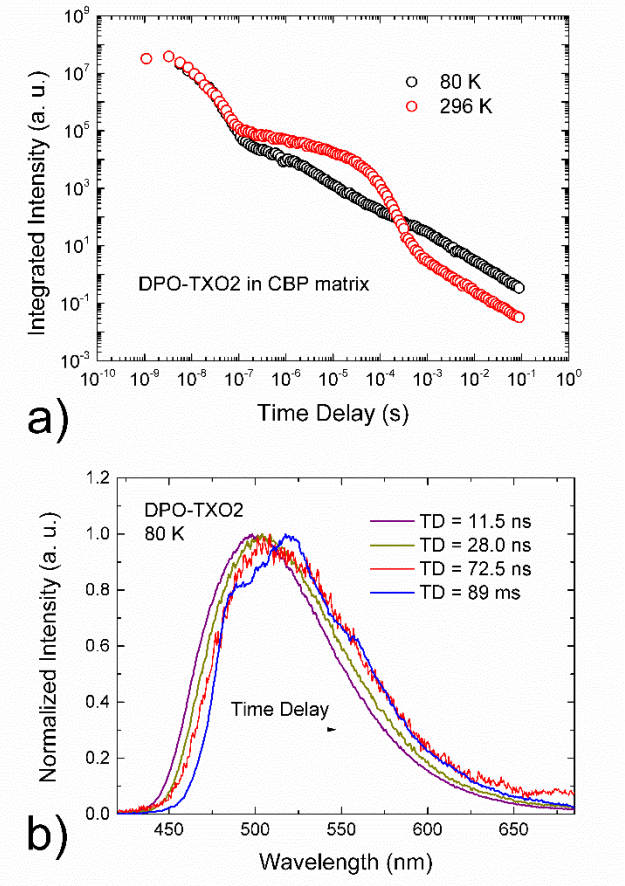

Fig. 10 a) Time resolved fluorescence decay of DPO-TXO2 in CBP matrix. The curves were obtained with 355 nm excitation. b) Time resolved normalized emission spectra in the entire region of analyses.

Figure 11 shows the full pathways available in molecules dispersed the two different environments in solid state, CBP and zeonex matrix. All the energy levels were taken by the onset of the spectra at 80 K apart from the ^3LE_D in CBP matrix. The mechanism responsible for the delayed fluorescence in both cases is TADF. In zeonex, ^3LE_D is located (slightly) above ^1CT, an unusual configuration. In the CBP matrix, ^3LE_D excitons are quenched by the triplet level of CBP and the radiative transition $^3LE_{CBP} \rightarrow S_0$ was observed strongly, which we assume indicates that in CBP matrix ^3LE_D is below ^1CT. In these two cases, the ^1CT level shows a strong energy shift (as in toluene compared to MCH solutions), leading to a difference of energy splitting between ^1CT and ^3LE_D. The host CBP is more polar than zeonex, a characteristic confirmed by the lower ^1CT level in this matrix.

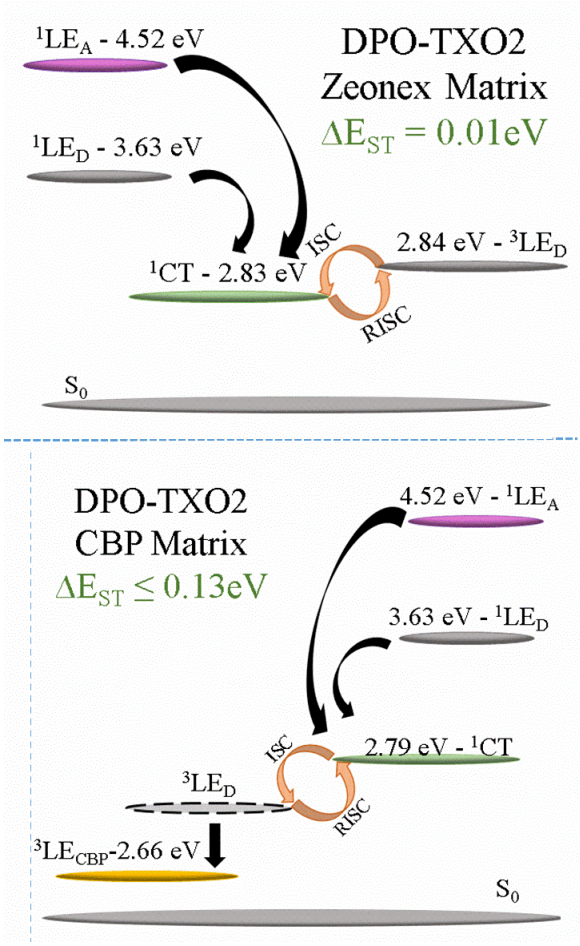

Fig. 11 Energy levels diagram describing the excited dynamics of DPO-TXO2 in zeonex and CBP matrix, evidencing the localized and charge transfer states.

Device performance

To evaluate the potential of DPO-TXO2 in OLEDs, we produced devices in two different hosts, CBP and bis[2-(di-(phenyl)phosphino)-phenyl]ether oxide (DPEPO). The latter has a reported higher triplet level (2.99 eV)[29] than CBP. The architecture of the devices was: ITO/NPB(40nm)/10%DPOTXO2:CBP(20nm)/ TPBi(60nm)/LiF/Al and NPB(40nm)/TCBPA(10nm)/ 10%DPO-TXO2:DPEPO(30nm)/TPBi(60nm)/LiF/Al. NPB is *N,N'*-bis(naphthalene-1-yl)-*N,N'*-bis(phenyl)-benzidine, TPBi is 1,3,5-tris(*N*-phenylbenzimidazol-2-yl)benzene) and TCBPA is 4,4 –(diphenymethylene)bis(*N,N*-diphenylaniline). The devices showed a maximum external quantum efficiency (E.Q.E.) of 6.5% at 8.3 cd/m^2 luminance and 13.5% at 166 cd/m^2 for CBP and DPEPO hosts, respectively. Both have green emission.

The photophysical analyses of DPO-TXO2:CBP thin film showed a strong quenching of excitons by the CBP host, due to its triplet level being the lowest energy pathway available in the system. Thus, CBP is not an appropriate host for DPO-TXO2 and it explains most of the low E.Q.E found in this device. The second device shows a strong increase in the E.Q.E value, due the triplet level of DPEPO located above the DPO-TXO2 energy levels, being an appropriate host for DPO-TXO2.

Figure 12a shows the E.Q.E *versus* current density curves and also the structure of the optimised device. Figure 12b shows its EL emission. The current density and brightness *versus* bias curves for both devices are shown in figure S8, ESI†. Therefore, the DPEPO device shows good E.Q.E values, high brightness levels >10,000 cd/m^2 and excellent resistance to roll- off up to 11 mA/cm^2.

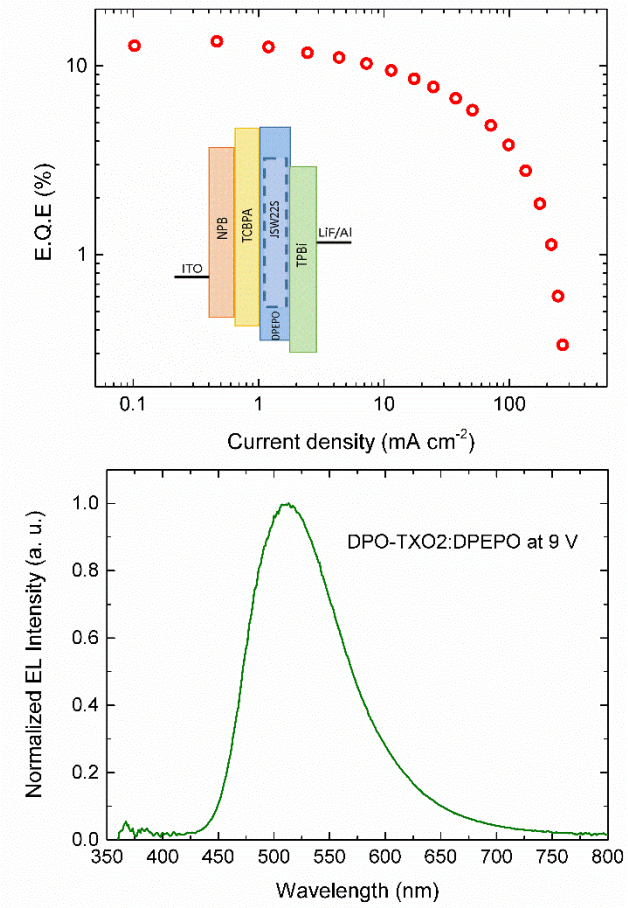

Fig. 12 a) E.Q.E versus Current density and structure of the devices b) EL spectra of DPO-TXO2:DPEPO OLED.

Conclusions

We report the design, synthesis and photophysical properties of the new TADF emitter molecule, 2,7-bis(phenoxazin-10-yl)-9,9-dimethylthioxanthene-*S,S*-dioxide (DPO-TXO2) dispersed in four different environments, along with the photophysics of the constituent phenoxazine and 9,9-dimethylthioxanthene-S,S-dioxide, donor and acceptor units of the DPO-TXO2. The DPO-TXO2 shows a strong and clear CT state, and the TADF was readily identified in solution and in solid state, giving rise to strong delayed emission.

In less polar environments (i.e. MCH solution and zeonex film) similar photophysics is observed. Both showed a small contribution of ^{1}LE$_D$ (donor singlet) emission in steady state measurements, as well as the ^{1}CT emission. Furthermore, they show a slow charge transfer step in the time resolved measurements indicative of weak electronic coupling between the donor and molecular CT state. The ^{1}LE$_D$ was observed at early times followed by monotonic stabilisation of ^{1}CT emission. In more polar environments, i.e., toluene solution and CBP matrix, only the ^{1}CT emission was identified in the steady state measurements and at early times in the time resolved measurements indicating much faster electron transfer (or more probably stabilisation of the charge separated character of the excited state). Also, we could identify a quenching of ^{3}LE$_D$ excitons by the CBP host, due to its triplet level being the lowest energy pathway available in the system. In a higher triplet host, DPEPO, very promising device performance is seen, showing maximum E.Q.E value of 13.5%, high brightness levels >10,000 cd/m^2 and excellent resistance to roll-off up to 11 mA/cm^2.

In polar and non-polar environments, it was shown that the ISC/RISC processes occur between ^{1}CT and ^{3}LE$_D$. This characteristic is essential to understand the energy difference of ΔE_{ST} depending on the environment. The ΔE_{ST} in MCH solution, toluene solution, zeonex matrix and CBP matrix were identified to be: (0.16±0.03) eV, (0.07±0.03) eV, (0.01±0.03) eV and $\leq$ 0.13 eV, respectively, showing the same TADF emitter displays distinct energy splitting between singlet and triplet states. We show that the environmental stabilisation of the ^{1}CT energy is responsible for the changing in ΔE_{ST}, since the ^{3}LE$_D$ remains the same, except in small molecule matrices where close packing has an effect on both singlet and triplet states. Even in solid state, where the polarity difference was small, the host brought a change in the ^{1}CT level, showing that the ^{1}CT state is strongly depend on the environment. Thus, it is possible to control the ΔE_{ST} by changing the host, and consequently, maximize the TADF mechanism. Therefore, efficient TADF can occur either in polar or in non-polar environments, because the crucial feature is where the ^{1}CT energy level lies with respect to the ^{3}LE (donor or acceptor) level. This explains why some TADF materials show stronger TADF in non-polar and others in polar environment. The polarity of the environment will clearly interfere in the stabilization of the CT formation. It was also demonstrated here that the ISC/RISC processes occur if the singlet state is localized at lower energy than the triplet state. Hence, excitons gaining thermal energy while they are in the singlet state to become isoenergetic with the local triplet level leads to spin orbit coupling causing crossing to the local triplet manifold, not just when they are in the triplet levels, as commonly believed in the TADF mechanism reported to date.

Overall, this study makes important contributions towards understanding principles of the underlying mechanism of TADF emitters and how many factors must be considered when designing a new TADF emitter. Firstly, we show that the environment has a key role in the energy level of ^{1}CT, which can be used to control the ΔE_{ST}. We show that it is critical to engineer the ^{1}CT state to be close in energy to a local donor or acceptor triplet state to mediate SOC and the TADF process, and that TADF can still occur when the local triplet state lies above the CT.

Acknowledgements

P. L. Santos thanks CAPES Foundation, Ministry of Education of Brazil, Brasilia - DF 70040 - 020, Brazil, in particular the Science Without Borders Program for PhD studentship, Proc. 12027/13-8. P. L. dos Santos also thanks Dr. Hameed A. Al Attar and Dr. Heather Cole for help with OLED production. J. S. Ward thanks EPSRC for funding. All authors thank EPSRC grant EP/L02621X/1.

References

1 C. W. Tang and S. A. Vanslyke, *Appl. Phys. Lett.*, 1987, **51**, 913–915.

2 Y. Im and J. Y. Lee, *Chem. Mater.*, 2014, **26**, 1413–1419.

3 T. Higuchi, H. Nakanotani and C. Adachi, *Adv. Mater.*, 2015, **27**, 2019–2023.

4 V. Jankus, P. Data, D. Graves, C. McGuinness, J. Santos, M. R. Bryce, F. B. Dias and A. P. Monkman, *Adv. Funct. Mater.*, 2014, **24**, 6178–6186.

5 F. B. Dias, K. N. Bourdakos, V. Jankus, K. C. Moss, K. T. Kamtekar, V. Bhalla, J. Santos, M. R. Bryce and A. P. Monkman, *Adv. Mater.*, 2013, **25**, 3707–3714.

6 H. Uoyama, K. Goushi, K. Shizu, H. Nomura and C. Adachi, *Nature*, 2012, **492**, 234–8.

7 Q. Zhang, B. Li, S. Huang, H. Nomura, H. Tanaka and C. Adachi, *Nat. Photonics*, 2014, **8**, 326–332.

8 H. Wang, L. Xie, Q. Peng, L. Meng, Y. Wang, Y. Yi and P. Wang, *Adv. Mater.*, 2014, **26**, 5198–5204.

9 F. B. Dias, *R. Soc.*, 2015, **373**, 20140447.

10 Q. Zhang, H. Kuwabara, W. J. Potscavage, S. Huang, Y. Hatae, T. Shibata and C. Adachi, *J. Am. Chem. Soc.*, 2014, **136**, 18070–18081.

11 H. Tanaka, K. Shizu, H. Nakanotani and C. Adachi, *Chem. Mater.*, 2013, **25**, 3766–3771.

12 T. Nakagawa, S.-Y. Ku, K.-T. Wong and C. Adachi, *Chem. Commun.*, 2012, **48**, 9580–9582.

13 B. T. Lim, S. Okajima, A. K. Chandra and E. C. Lim, *Chem. Phys. Lett.*, 1981, **79**, 22–27.

14 Z. E. X. Dance, S. M. Mickley, T. M. Wilson, A. B. Ricks, A. M. Scott, M. A Ratner and M. R. Wasielewski, *J. Phys. Chem. A*, 2008, **112**, 4194–4201.

15 I. R. Gould, J. a Boiani, E. B. Gaillard, J. L. Goodman and S. Farid, *J. Phys. Chem. A*, 2003, **107**, 3515–3524.

16 J. Lee, K. Shizu, H. Tanaka, H. Nomura, T. Yasuda and C. Adachi, *J. Mater. Chem. C*, 2013, **1**, 4599.

17 X.-K. Chen, S.-F. Zhang, J.-X. Fan and A.-M. Ren, *J. Phys. Chem. C*, 2015, **119**, 9728–9733.

18 A. P. Kulkarni, Y. Zhu, A. Babel, P. T. Wu and S. A. Jenekhe, *Chem. Mater.*, 2008, **20**, 4212–4223.

19 A. Nowakowska-Oleksy, J. Sołoducho and J. Cabaj, *J. Fluoresc.*, 2011, **21**, 169–178.

20 T. Okamoto, M. Kozaki, M. Doe, M. K. Toshihiro Okamoto Matsumi Doe Manabu Uchida Guofang Wang, K. Okada, M. Uchida and G. Wang, *Chem. Mater.*, 2005, **17**, 5504–5511.

21 H. Tanaka, K. Shizu, H. Miyazaki and C. Adachi, *Chem. Commun.*, 2012, **48**, 11392.

22 T. Ogiwara, Y. Wakikawa and T. Ikoma, *J. Phys. Chem. A*, 2015, **119**, 3415–3418.

23 Q. Zhang, J. Li, K. Shizu, S. Huang, S. Hirata, C. Adachi, P. C. Adachi, Q. Zhang, J. Li, K. Shizu, S. Hirata and H. Miyazaki, *J. Am. Chem. Soc.*, 2012, **134**, 14706–9.

24 J. R. Huber and W. W. Mantulin, *J. Am. Chem. Soc.*, 1972, **94:11**, 3755–3760.

25 F. I. Mopsik, *J. Chem. Phys.*, 1969, **50**, 2559–2569.

26 J. Lee, K. Shizu, H. Tanaka, H. Nakanotani, T. Yasuda, H. Kaji and C. Adachi, *J. Mater. Chem. C*, 2015, **3**, 2175–2181.

27 P. Schrögel, A. Tomkevičienė, P. Strohriegl, S. T. Hoffmann, A. Köhler and C. Lennartz, *J. Mater. Chem.*, 2011, **21**, 2266–2273.

28 V. Jankus, C. Winscom and A. P. Monkman, *J. Chem. Phys.*, 2009, **130**, 074501.

29 H. Xu, L.-H. Wang, X.-H. Zhu, K. Yin, G.-Y. Zhong, X.-Y. Hou and W. Huang, *J. Phys. Chem. B*, 2006, **110**, 3023–9.